PIER M

Screen Printed High Gain EBG-Based Wearable Textile Antenna for Wireless Medical Band Applications

Somasundaram Arulmurugan, TR Suresh Kumar*, and Zachariah C. Alex

School of Electronics Engineering, Vellore Institute of Technology, Vellore, Tamilnadu, India

ABSTRACT: A screen-printed wearable coplanar waveguide (CPW) fed semi-octagonal shaped antenna is developed on a denim textile substrate to resonate at 2.45 GHz for wireless medical body area network communications. The antenna is integrated with a circular ring-type electromagnetic bandgap structure (EBG) to mitigate performance degradation due to the high permittivity of the tissue model when it works on body conditions. The CPW antenna and EBG surfaces are fabricated using the screen-printing method, which provides good conformability, good wearable comfortability, and light weight. The proposed EBG integrated antenna has dimensions of $0.66\lambda \times 0.66\lambda \times 0.056\lambda$ and an impedance bandwidth of 13% (2.3–2.62 GHz) with a gain of 6.7 dB. The specific absorption rates (SARs) of the antenna are 0.309 W/kg and 0.14 W/kg for 1 g and 10 g of tissue, respectively, which are within the wearable safety limits. Thus, the fabricated prototype antenna is suitable for wearable WBAN and MBAN applications.

1. INTRODUCTION

Textile wearable antennas monitor various vital signs to diagnose the disease. Fabric-based wearable antennas provide better performance, improve desirability, and reduce wearable discomfort. Various fabrication techniques are involved in fabricating textile wearable antennas, such as adhesive, inkjet printing, weaving, embroidery, and screen printing. The majority of researchers have developed textile antennas based on the adhesive technique. In adhesive fabrication, conductive patterns are directly attached to the textile substrates using glue or adhesive paste, which reduces fabrication complexity. An inverted E-shaped patch structure with a partial ground plane [1] is developed on a denim substrate using the adhesive technique to resonate at 2.45 GHz. Due to partial ground, the antenna has a bidirectional radiation pattern, which leads to high SAR. A multilayer aperture-coupled textile antenna is attached to the felt and fleece substrate using adhesive fabrication, which operates at 2.45 GHz [2]. However, manually aligning multilayer aperture coupled portions such as patch, feedline, and aperture gap is difficult, has low precision, and may degrade the results. In [3], a textile wearable antenna with defective ground surface is developed on a polyester substrate to resonate at 2.45 GHz. The conductive portion of the radiating elements is made on copper foil tape and attached to the polyester substrate with the help of a self-adhesive paste. However, due to their poor durability and mechanical stability, copper foil and adhesive fabrication are not preferred for regular use [4]. In [5], an inkjet-printed wearable textile antenna is realized on polyester cotton substrates to resonate at 2.45 GHz. Before inkjet printing, a non-conductive ink is screen-printed in order to minimize the substrate surface roughness and to create a uniform surface for continuous conducting, but the combination of inkjet and screen-printing increases the fabrication complexity. A wearable antenna is embroidered on a cotton textile substrate to resonate at 2.45 GHz [6]. In embroidery fabrication, conductive patterns of patch and ground are realized on two separate substrates and stacked with nonconductive thread in order to avoid electrical shorting between patch and ground, which leads to an increase in size. Furthermore, the air gap between conductive thread stitches affects the surface conductivity and antenna performance. A wearable electro-textile multilayer woven patch antenna [7] was fabricated on a cotton substrate to operate at 2.45 GHz. In the weaving process [8], conductive yarns of the patch antenna should be arranged according to the major current flow direction to reduce back lobes and improve the gain.

However, additional procedures like cutting, sewing, and binding are required in the woven patch to complete the fabrication process. In [9], an E-shaped multilayer antenna is screen printed on polyvinyl butyral (PVB) coated polyester fabric to resonate at 3.37 GHz for WiMAX applications, with a 3.6 dB realized gain. PVB dip coating provides uniform fabric surfaces for conductive section printing and mitigates electromagnetic interference during water absorption. Cavity backed surface integrated waveguide (SIW) antennas are proposed [10, 11] which give high isolation between human body and antenna without large ground plane reflector. The limitation of SIW is difficult to fabricate vertical metallic vias in the sidewalls of textile substrate. Compared to adhesive, inkjet, weaving, embroidery, and SIW techniques, the screen-printing technique is chosen due to low-cost fabrication, precise structure realization, good wearable comfortability, and light weight. To improve the radiation efficiency and SAR reduction, the reflector is placed below the antenna with $\lambda/4$ distance to obtain in-phase reflection [12, 13] which leads to increased
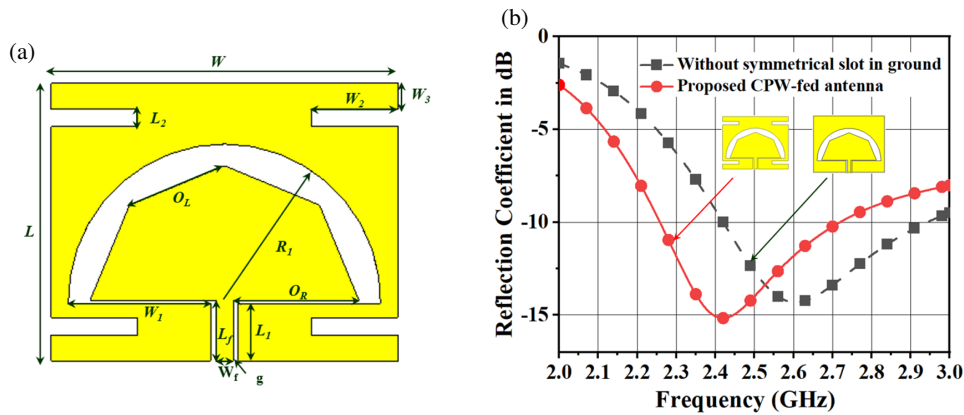
(a)

(b)

FIGURE 1. (a) Schematic diagram of proposed circular slot semi octagonal shaped antenna. [The optimized antenna dimensions are $L = 32$, $W = 40$, $R_1 = 18$, $O_L = 11.86$, $W_1 = 16.4$, $L_1 = 6$, $L_2 = 2$, $g = 0.6$, $W_3 = 3$, $L_f = 7$, and $W_f = 2$, all dimensions in mm]. (b) Simulated S_{11} results of proposed CPW antenna.

antenna thickness. To miniaturize the reflector height and improve the wearable comfortability, a circular porous EBG structure is developed on a denim substrate [14]. However, porous ground may allow to observe moisture and sweat, which may degrade antenna performance. In [15], an eight-shaped EBG structure is developed on a denim substrate and integrated with a monopole antenna to improve the bandwidth. However, these structures increase the area. In order to resolve this issue, a uniplanar circular ring EBG structure is proposed. The proposed work focuses on a screen-printed fabric antenna integrated with an EBG structure for WBAN and MBAN applications. The proposed EBG structure provides in-phase reflection characteristics at 2.45 GHz, which enhances the gain and consequently reduces the back radiation and SAR.

2. ANTENNA DESIGN

2.1. CPW-Fed Textile Wearable Antenna Design

The wearable CPW antenna consists of a semicircular ring-slotted ground plane with a semi-octagonal shaped stub. The conductive portion of the antenna is a screen printed on one side of a 1.4 mm thick denim (jean) fabric substrate, as shown in Figure 1(a). The dielectric constant (ε_r) of denim is 1.7, and the loss tangent ($\tan \delta$) is 0.025 [16]. The semi-octagon-shaped structure is used as a tuning stub, which is surrounded by a semicircular ring-slotted ground plane. The antenna resonates at 2.6 GHz when the perimeter of the semicircular slot is about the one guided wavelength ($\lambda_g = 92.5$ mm) of the 50-ohm CPW feed line [17]. Furthermore, introducing symmetrical horizontal slots in the ground helps to shift the antenna frequency from 2.6 to 2.4 GHz, as shown in Figure 1(b). The semi-octagon-shaped stub is symmetrical with respect to the feed, which reduces the high impedance of the semicircular slot and matches with 50-ohm impedance.

The CPW-fed semi-octagon-shaped structure exhibits a bidirectional radiation pattern which leads to the increase in SAR. Moreover, when the antenna operates close to the human body, it detunes the frequency due to the high permittivity of the human tissue model. Therefore, it is essential to separate the mod-

eled antenna from human tissue. To overcome these problems, a 3×3 uniplanar circular ring EBG array is designed to be kept at the bottom of the CPW-fed structure to mitigate the backward radiation, SAR, and to improve the forward gain.

2.2. Parametric Analysis

The key parameters of the proposed antenna's slotted radius (R_1), horizontal slot width (W_2), and semi-octagonal shaped stub dimension (O_L) are examined. It can be observed that increasing the R_1 value shifts the frequency to lower resonance due to the increase in the current path of the semicircular slot circumference, which is shown in Figure 2(a).

The semi-octagonal stub dimension is varied, and the effect of the reflection coefficient is observed in Figure 2(b). The stub dimension is optimized to obtain better impedance matching at 2.45 GHz.

Horizontal symmetrical slots (W_2) are etched on the ground plane to shift the resonance frequency from 2.6 to 2.4 GHz; when the slot width increases, the capacitance value increases; therefore, the resonance value shifts to lower, which is depicted in Figure 2(c).

2.3. Circular Ring EBG Design

The EBG structure consists of a circular ring array on one side of a 3 mm denim substrate and a ground structure on the other side, as shown in Figure 3(a). The designed EBG structure forms a 3×3 array on the rear side of the antenna to mitigate the backward radiation. The EBG characteristics are analyzed by plotting the reflection phase. Initially, the length and width of the EBG unit cell is $L_e = 28.5$ mm which is designed using a circular patch, creating 0° reflection phase at 3.5 GHz. Then the patch is cut with a circular slot of radius r_1, which offers 0° reflection phase at 2.45 GHz and helps to miniaturize the EBG unit cell. The inductance (L_s) is produced by the circular current loop in the ring surface, and the space between the two adjacent circular rings generates capacitance (C_s). The thickness of the substrate between the top and bottom layers is modeled as dielectric-loaded short-circuited transmission line inductance
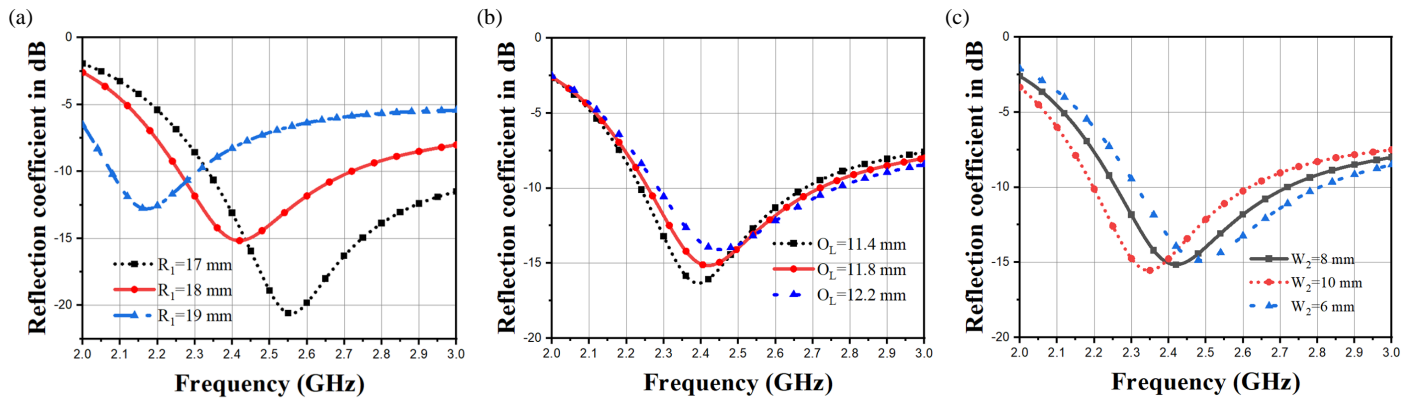
138

FIGURE 2. (a) Parametric analysis of R_1. (b) Parametric analysis of O_L. (c) Parametric analysis of W_2.
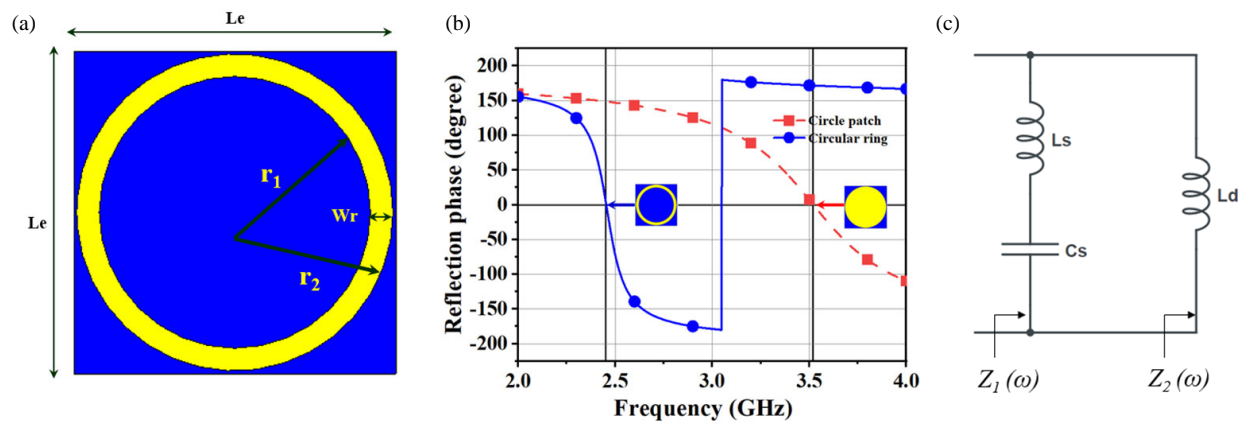

FIGURE 3. (a) Schematic diagram of single EBG unit cell. (b) Reflection phase of circular ring EBG unit cell model. [The optimized dimensions of circular ring EBG unit cell is $L_e = 28.5$, $W_r = 2$, $r_1 = 12$, $r_2 = 14$; all dimensions in mm]. (c) Equivalent circuit model of conventional circular patch EBG.

(L_d). The equivalent capacitance (C_S) of two adjacent circular rings is almost the same as circular patch EBG, and the equivalent inductance (L_s) of a circular ring increases compared with a circular patch because the current path increases in circumference. Therefore, the effect of increasing inductance (L_s) shifts the frequency from 3.5 to 2.45 GHz. The circumference of the circular ring EBG is about one wavelength $\lambda_o = 88$ mm, which is optimized to match zero reflection phase at center frequency 2.45 GHz, as shown in Figure 3(b). EBG structure behaves like an artificial magnetic conductor when the reflection phase crosses zero degrees. The reflection phase bandwidth is observed between $-90°$ and $90°$, which is 160 MHz from 2.37 to 2.53 GHz. The equivalent circuit diagram of a unit cell is depicted in Figure 3(c). The total surface impedance and resonant frequency of the EBG structure can be calculated using Eqs. (1) and (2) [18, 19].

$$Zs(\omega) = Z_1 \,||\, Z_2 = \frac{j\omega L_d(1 - \omega^2 L_s C_s)}{1 - \omega^2 C_s(L_s + L_d)} \quad (1)$$

$$f = \frac{1}{2\pi\sqrt{(L_s + L_d)C_s}} \quad (2)$$

3. INTEGRATION OF CPW-FED TEXTILE WEARABLE ANTENNA ON EBG STRUCTURE

The proposed CPW-fed textile wearable antenna is placed above the 3×3 circular ring-type EBG structure at a distance of 3 mm using a foam spacer, as shown in Figure 4(a). This foam spacer prevents the SubMiniature version A (SMA) connector from intersecting the EBG, as shown in Figure 4(b). EBG structure is used to avoid the frequency detuning due to the high dielectric constant of the human tissue model and reduce the SAR. Perfect electric conductor (PEC) reflector requires $\lambda/4$ distance to create null phase shift, but EBG structure provides zero phase shift without $\lambda/4$ distance. Owing to the EBG in-phase reflection characteristics, the antenna and image currents are constructively added to increase the antenna gain, as shown in Figure 4(c). The simulated reflection coefficient of the EBG integrated antenna structure lies in the frequency range of 2.4 to 2.51 GHz, which is depicted in Figure 5(a). Surface current is symmetrically distributed through the antenna along the y-axis with respect to feed. In the x-axis, the current is equal and 180-degree out of phase, which is seen in Figure 5(b).

The SAR validation is performed using the human Hugo voxel model and simplified multi-layer tissue model. Initially,
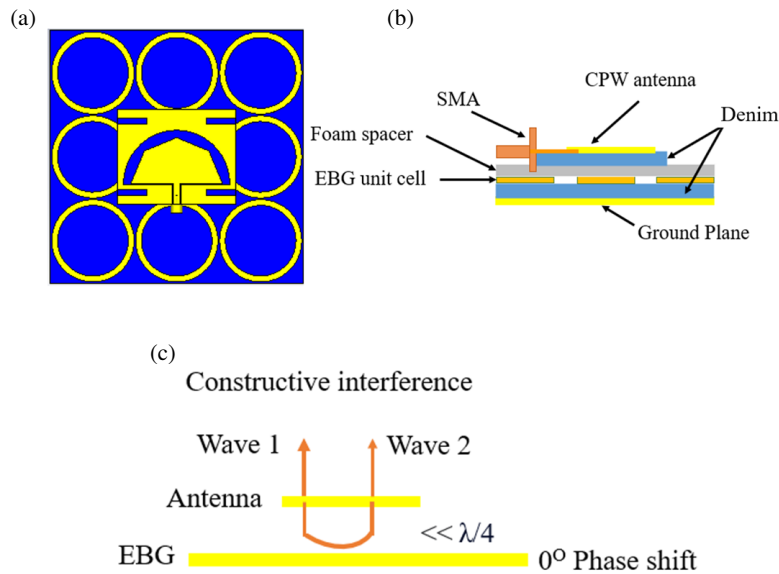
FIGURE 4. (a) EBG integrated CPW-fed antenna. (b) Side view of the proposed structure. (c) Antenna on EBG surface.
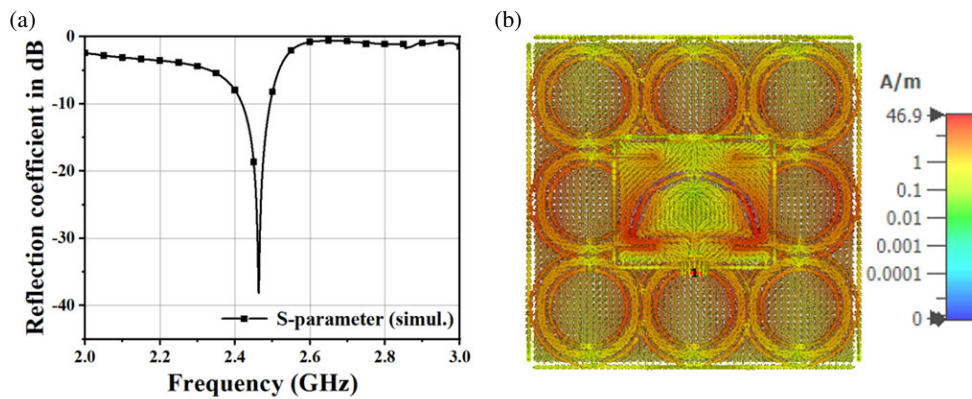

FIGURE 5. (a) Reflection coefficient of EBG integrated structure. (b) Surface current distribution with EBG.

TABLE 1. Properties of human tissue models.

Phantom	Freq = 2.45 GHz		Density	Thickness
Layers	ε_r	σ (S/m)	(kg/m^3)	(mm)
Skin	37.95	1.49	1001	3
Fat	5.27	0.11	900	7
Muscle	52.67	1.77	1006	20
Bone	18.49	0.82	1008	10

the EBG integrated antenna is placed on the human chest at a 3 mm distance to validate the SAR performance. The maximum SAR value is 0.0819 W/kg for 1 g tissue obtained on the human Hugo chest voxel model, which is shown in Figures 6(a) & (b). Furthermore, the proposed antenna is positioned on the four-layer human phantom tissue model on the surface and validated SAR value, as shown in Figure 6(c). The properties of the multi-layer tissue model are shown in Table 1. According to the European Union (EU) and FCC guidelines [20], the SAR value is always less than 2 W/kg (10 gram) and 1.6 W/kg (1 gram) tis-

sue model. The SAR value of the proposed EBG integrated antenna well meet the EU and Federal Communications Commission (FCC) wearable safety limit. The SAR performance o with and without EBG structure is shown in Table 2. The fundamental calculation of SAR evaluation is shown in Eq. (3), where E represents the electric field (V/m), σ the conductivity (S/m), and ρ the mass density of the tissue (kg/m^3).

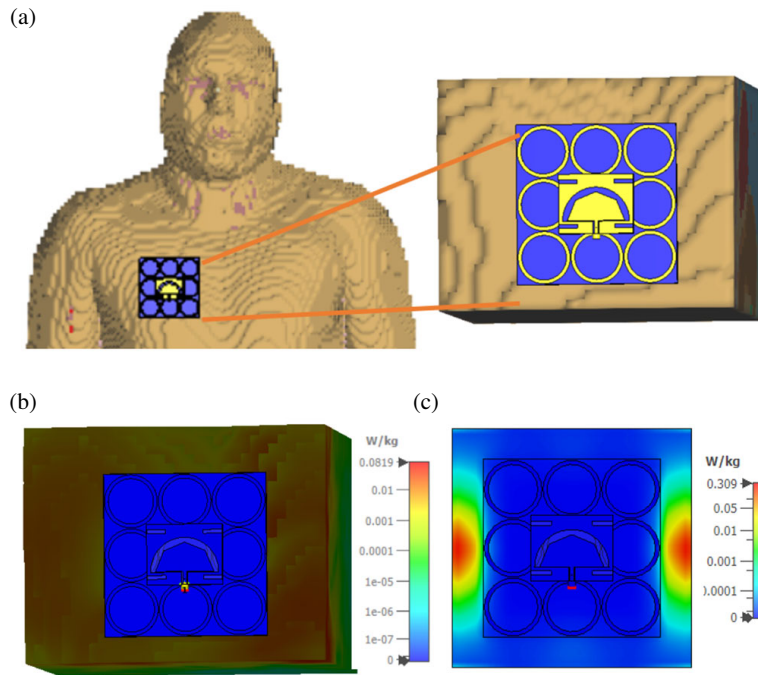$$SAR = \frac{\sigma |E|^2}{\rho} \tag{3}$$

FIGURE 6. (a) Antenna placement human Hugo voxel model. (b) SAR performance of Hugo voxel model. (c) SAR evaluation on four-layer phantom tissue model at 2.45 GHz.
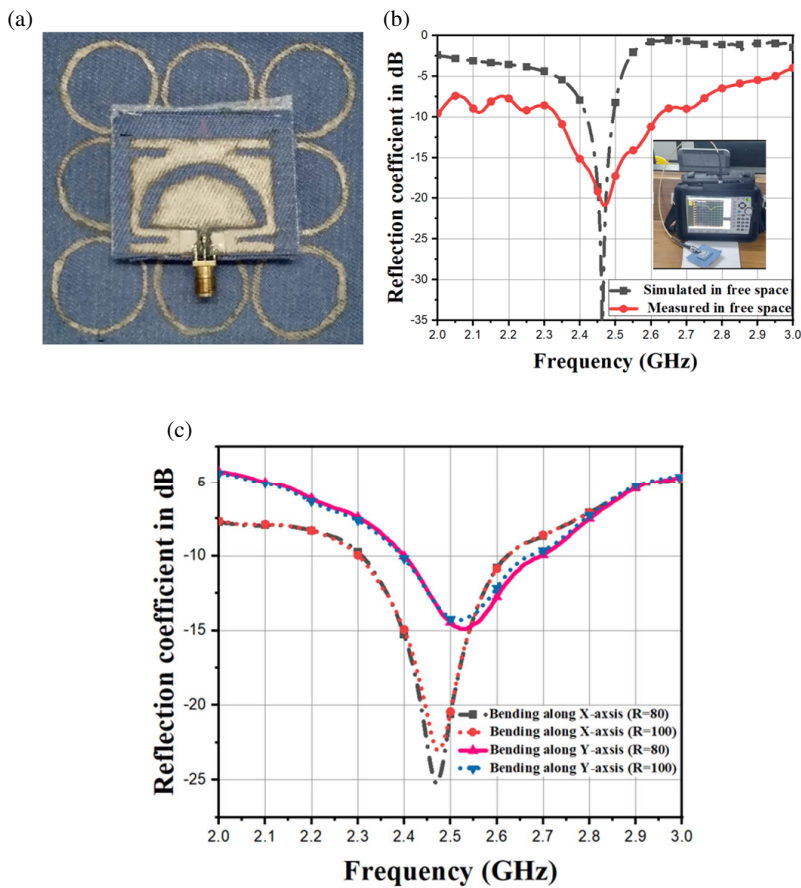

FIGURE 7. (a) Screen printed prototype model. b) Simulated vs measured S_{11} results of proposed EBG integrated with CPW antenna. (c) Bending analysis.
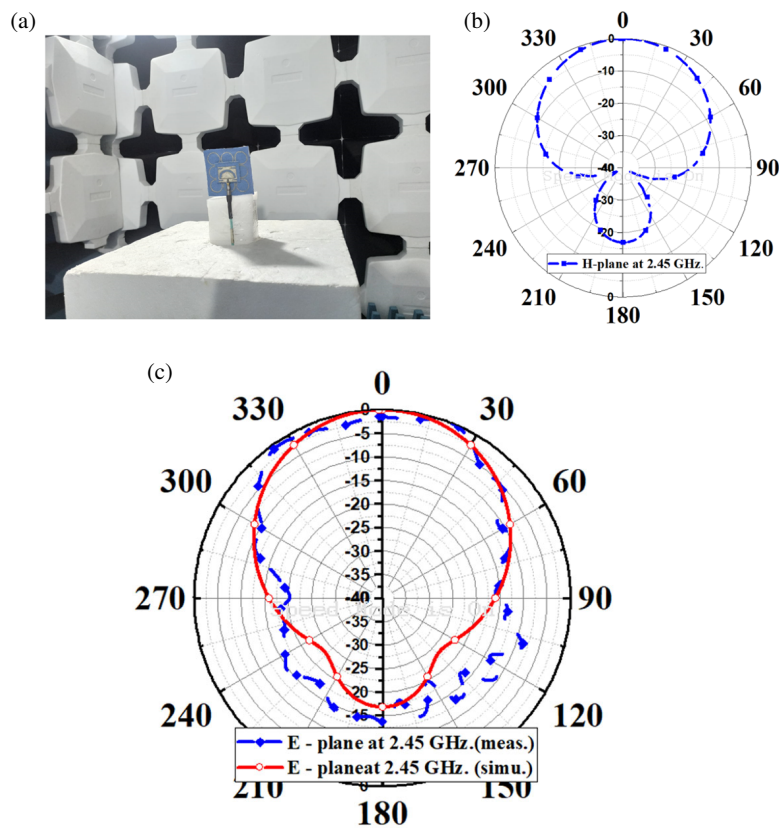
(a)

(b)

(c)

FIGURE 8. (a) Radiation pattern measurement. (b) H-plane radiation pattern at 2.45 GHz. (c) Measured and simulated E-plane at 2.45 GHz.

TABLE 2. SAR comparison without and with EBG structure.

SAR analysis at 2.45 GHz (W/kg)		
Multilayer tissue	**1 gram**	**10 grams**
CPW-fed antenna without EBG	32	19
EBG integrated CPW-fed antenna	0.309	0.140

4. FABRICATION AND MEASUREMENT

4.1. Screen Printing

Wearable antennas must be lightweight, conformal, durable, mechanically stable, and easily integrated with textile material. To satisfy these requirements, a conductive screen-printing technique is adopted here to fabricate a wearable antenna. The conductive portion of the CPW-fed antenna and circular ring type EBG structure are printed on denim cloth by using silver conductive ink (surface resistance of 0.01 Ω/sq) which is shown in Figure 7(a). Initially, the screen-printing mask is prepared where non-conductive portions are masked by using emulsion, and conductive portions are left open on the screen [21]. The conductive ink is applied above the screen and pushed through the squeeze, and the printed structure is cured at 110°C. An SMA connector is surface-mounted on the CPW antenna using silver epoxy conductive paste.

4.2. Measurement

An Anritsu MS2027C Vector Network Analyzer (VNA) is used to measure the return loss in flat and various radius bent conditions along with the y and x axes to ensure the frequency sustained during the on-body realistic condition. The measured and simulated EBG integrated antenna reflection coefficients are shown in Figure 7(b), covering the frequency range of 2.3–2.62 GHz along with 320 MHz bandwidth. The return loss of the EBG integrated antenna in various bent radius is shown in Figure 7(c), where the frequency and bandwidth are slightly shifted compared with the flat condition. When the antenna is bent according to the x-axis, the width of the antenna affects the input impedance. Therefore, the return loss is higher than the flat conditions. However, in bending conditions, the proposed antenna still maintains an S_{11} result of less than -10 dB between 2.44 and 2.6 GHz.

The radiation pattern of the screen-printed EBG-integrated CPW-fed antenna is validated through an anechoic chamber, which is depicted in Figure 8(a). Without the EBG structure, the antenna has a 2.06 dB peak gain; when the antenna is attached to the 3×3 circular ring-type EBG structure, it has a maximum gain of 6.7 dB. EBG structures behave like a perfect magnetic conductor (PMC) at 2.45 GHz (null reflection phase); therefore, the back radiation is reflected back in the forward direction with in-phase reflection and enhances the forward gain by 4.6 dB.

Figures 8(b) and (c) show the normalized H-plane and E-plane radiation patterns at 2.45 GHz. The purposive EBG inte-

TABLE 3. Comparison of proposed screen-printed wearable antenna with literature works.

Ref.	Substrate	Permittivity	Freq. (GHz)	BW (%)	Gain (dB)	Fabrication	Area
[22]	Fleece	1.2	2.45	9.52	7	Adhesive	$(2.4 \times 1.6 \times 0.05)\lambda$
[23]	Felt	1.4	2.45	4	2.42	Adhesive	$(0.8 \times 0.8 \times 0.048)\lambda$
[24]	Felt	1.2	2.45	15	7.3	Adhesive	$(0.66 \times 0.66 \times 0.032)\lambda$
[25]	Jean	1.7	2.4	8.3	6.5	Adhesive	$(0.48 \times 0.48 \times 0.019)\lambda$
[16]	Jean	1.7	2.45	12	3.5	Adhesive	$(0.3 \times 0.15 \times 0.0023)\lambda$
[26]	Jean	1.7	2.45	32	6.4	Adhesive	$(0.48 \times 0.48 \times 0.019)\lambda$
[6]	Cotton	1.7	2.45	1	5.25	Embroidery	$(0.40 \times 0.4 \times 0.008)\lambda$
[27]	Cotton	1.5	2.45	20	7.1	Embroidery	$(0.93 \times 1.00 \times 0.016)\lambda$
[28]	Felt	1.4	2.45	6	5.35	SIW	$(0.61 \times 0.39 \times 0.02)\lambda$
[29]	Jean	1.7	2.45	22	8.3	Adhesive	$(1.128 \times 1.128 \times 1.1)\lambda$
Proposed	Denim	1.7	2.45	13	6.7	Screen printing	$(0.66 \times 0.66 \times 0.05)\lambda$

grated antenna has a unidirectional radiation pattern with measured and simulated gains of 6.7 and 7.1 dB, respectively, and has a front-back ratio of 16.9 dB. The proposed EBG-based textile wearable antenna performance is compared with the existing textile substrate-based wearable antenna reported in terms of fabrication technique, bandwidth, gain, and area at 2.45 GHz, as listed in Table 3. It shows that the proposed screen-printed antenna has a gain of 6.7 dB and 13% impedance bandwidth with a miniaturized antenna size, which is better than the existing works.

5. CONCLUSION

A wearable screen-printed semi-octagonal CPW-fed antenna combined with an EBG structure is presented for wireless medical band communications at 2.45 GHz. The 3×3 circular ring screen-printed EBG array is incorporated with a CPW-fed antenna to eliminate the impedance mismatch and SAR reduction when it operates closer to the human tissue model. The proposed screen-printed structure has a dimension of $0.66\lambda \times 0.66\lambda \times 0.056\lambda$, and the impedance bandwidth of (2.3–2.62 GHz) 13% with a 6.7 dB gain is observed. The resonant frequencies are stable under various bending radii, which is suitable for flexible applications. In addition, the SAR value is obtained to be 0.309 (1 gram) and 0.14 (10 gram) W/kg for tissue, which satisfies FCC and EU specifications for wearable applications.

ACKNOWLEDGEMENT

REFERENCES

[1] Ashyap, A. Y. I., Z. Z. Abidin, S. H. Dahlan, H. A. Majid, A. M. A. Waddah, M. R. Kamarudin, G. A. Oguntala, R. A. Abd-Alhameed, and J. M. Noras, "Inverted E-shaped wearable textile antenna for medical applications," *IEEE Access*, Vol. 6, 35 214–35 222, 2018.

[2] Hertleer, C., A. Tronquo, H. Rogier, L. Vallozzi, and L. V. Langenhove, "Aperture-coupled patch antenna for integration into wearable textile systems," *IEEE Antennas and Wireless Propagation Letters*, Vol. 6, 392–395, 2007.

[3] Harris, H. A., R. Anwar, Y. Wahyu, M. I. Sulaiman, Z. Mansor, and D. A. Nurmantris, "Design and implementation of wearable antenna textile for ISM band," *Progress In Electromagnetics Research C*, Vol. 120, 11–26, 2022.

[4] Somasundaram, A., S. K. T. Rajamanickam, and Z. C. Alex, "Development of wideband CPW-fed microstrip patch antenna on textile substrate," *Microwave and Optical Technology Letters*, Vol. 65, No. 8, 2352–2358, Aug. 2023.

[5] Whittow, W. G., A. Chauraya, J. C. Vardaxoglou, Y. Li, R. Torah, K. Yang, S. Beeby, and J. Tudor, "Inkjet-printed microstrip patch antennas realized on textile for wearable applications," *IEEE Antennas and Wireless Propagation Letters*, Vol. 13, 71–74, 2014.

[6] Anbalagan, A., E. F. Sundarsingh, V. S. Ramalingam, A. Samdaria, D. B. Gurion, and K. Balamurugan, "Realization and analysis of a novel low-profile embroidered textile antenna for real-time pulse monitoring," *IETE Journal of Research*, Vol. 68, No. 6, 4142–4149, Nov. 2022.

[7] Sundarsingh, E. F., M. Kanagasabai, and V. S. Ramalingam, "Completely integrated multilayered weave electro-textile antenna for wearable applications," *International Journal of Microwave and Wireless Technologies*, Vol. 9, No. 10, 2029–2036, Dec. 2017.

[8] Xu, F., L. Yao, D. Zhao, M. Jiang, and Y. Qiu, "Effect of weaving direction of conductive yarns on electromagnetic performance of 3D integrated microstrip antenna," *Applied Composite Materials*, Vol. 20, No. 5, 827–838, Oct. 2013.

[9] Roshni, S. B., M. P. Jayakrishnan, P. Mohanan, and K. P. Surendran, "Design and fabrication of an E-shaped wearable textile antenna on PVB-coated hydrophobic polyester fabric," *Smart Materials and Structures*, Vol. 26, No. 10, 105011, Oct. 2017.

[10] Çelenk, E. and N. T. Tokan, "All-textile on-body antenna for military applications," *IEEE Antennas and Wireless Propagation Letters*, Vol. 21, No. 5, 1065–1069, May 2022.

[11] Casula, G. A., G. Montisci, and G. Muntoni, "A novel design for dual-band wearable textile eighth-mode SIW antennas," *IEEE Access*, Vol. 11, 11 555–11 569, 2023.

[12] Shah, A. and P. Patel, "Broadband coplanar waveguide-fed stub loaded pot shape E-textile antenna equipped with perfect electric conductor," *International Journal of RF and Microwave Computer-Aided Engineering*, Vol. 31, No. 5, 608–614, May 2021.

[13] Ullah, U., I. B. Mabrouk, and S. Koziel, "A compact circularly polarized antenna with directional pattern for wearable off-body communications," *IEEE Antennas and Wireless Propagation Letters*, Vol. 18, No. 12, 2523–2527, Dec. 2019.

[14] Sandhya, M. and L. Anjaneyulu, "Improved wearable, breathable, triple-band electromagnetic bandgap-loaded fractal antenna for wireless body area network applications," *ETRI Journal*, 1–10, May 2023.

[15] Keshwani, V. R., P. P. Bhavarthe, and S. S. Rathod, "Eight shape electromagnetic band gap structure for bandwidth improvement of wearable antenna," *Progress In Electromagnetics Research C*, Vol. 116, 37–49, 2021.

[16] Singh, S. and S. Verma, "Printed compact asymmetric dual L-strip fed split-ring shaped EBG-based textile antenna for WBAN applications," *Microwave and Optical Technology Letters*, Vol. 62, No. 12, 3897–3904, 2020.

[17] Saeed, S. M., C. A. Balanis, and C. R. Birtcher, "Inkjet-printed flexible reconfigurable antenna for conformal WLAN/WiMAX wireless devices," *IEEE Antennas and Wireless Propagation Letters*, Vol. 15, 1979–1982, 2016.

[18] Li, G., H. Zhai, L. Li, C. Liang, R. Yu, and S. Liu, "AMC-loaded wideband base station antenna for indoor access point in MIMO system," *IEEE Transactions on Antennas and Propagation*, Vol. 63, No. 2, 525–533, Feb. 2015.

[19] Amjadi, S. M. and M. Soleimani, "A novel compact artificial magnetic conductor based on multiple non-grounded vias," *PIERS Online*, Vol. 2, No. 6, 672–675, 2006.

[20] I. S. C. C. 28, IEEE Standards Coordinating Committee, *IEEE Recommended Practice for Measurements and Computations of Radio Frequency Electromagnetic Fields with Respect to Human Exposure to Such Fields*, Vol. 2002, 2003.

[21] Yang, H. and X. Liu, "Screen-printed dual-band and dual-circularly polarized textile antenna for wearable applications," in *2021 15th European Conference on Antennas and Propagation (EuCAP)*, 1–4, 2021.

[22] Kamardin, K., M. K. A. Rahim, P. S. Hall, N. A. Samsuri, T. A. Latef, and M. H. Ullah, "Planar textile antennas with artificial magnetic conductor for body-centric communications," *Applied Physics A — Materials Science & Processing*, Vol. 122, No. 4, 1–9, 2016.

[23] Lago, H., P. J. Soh, M. F. Jamlos, N. Shohaimi, S. Yan, and G. A. E. Vandenbosch, "Textile antenna integrated with compact AMC and parasitic elements for WLAN/WBAN applications," *Applied Physics A — Materials Science & Processing*, Vol. 122, No. 12, 1–6, 2016.

[24] Gao, G.-P., B. Hu, S.-F. Wang, and C. Yang, "Wearable circular ring slot antenna with EBG structure for wireless body area network," *IEEE Antennas and Wireless Propagation Letters*, Vol. 17, No. 3, 434–437, Mar. 2018.

[25] Ashyap, A. Y. I., Z. Z. Abidin, S. H. Dahlan, H. A. Majid, M. R. Kamarudin, A. Alomainy, R. A. Abd-Alhameed, J. S. Kosha, and J. M. Noras, "Highly efficient wearable CPW antenna enabled by EBG-FSS structure for medical body area network applications," *IEEE Access*, Vol. 6, 77 529–77 541, 2018.

[26] Ashyap, A. Y. I., S. H. B. Dahlan, Z. Z. Abidin, M. H. Dahri, H. A. Majid, M. R. Kamarudin, S. K. Yee, M. H. Jamaluddin, A. Alomainy, and Q. H. Abbasi, "Robust and efficient integrated antenna with EBG-DGS enabled wide bandwidth for wearable medical device applications," *IEEE Access*, Vol. 8, 56 346–56 358, 2020.

[27] Anbalagan, A., E. F. Sundarsingh, and V. S. Ramalingam, "Design and experimental evaluation of a novel on-body textile antenna for unicast applications," *Microwave and Optical Technology Letters*, Vol. 62, No. 2, 789–799, Feb. 2020.

[28] Lajevardi, M. E. and M. Kamyab, "Ultraminiaturized metamaterial-inspired SIW textile antenna for off-body applications," *IEEE Antennas and Wireless Propagation Letters*, Vol. 16, 3155–3158, 2017.

[29] Sugumaran, B., R. Balasubramanian, and S. K. Palaniswamy, "Performance evaluation of compact FSS-integrated flexible monopole antenna for body area communication applications," *International Journal of Communication Systems*, Vol. 35, No. 6, 1–18, Apr. 2022.